

Constraining mass-transfer and common-envelope physics with post-supernova companion monitoring

Ryosuke Hirai^{1,2}★

¹ *School of Physics and Astronomy, Monash University, Clayton, Victoria 3800, Australia*

² *OzGrav: The ARC Centre of Excellence for Gravitational Wave Discovery, Australia*

Accepted XXX. Received YYY; in original form ZZZ

ABSTRACT

We present an analytical model that describes the response of companion stars after being impacted by a supernova in a close binary system. This model captures key properties of the luminosity evolution obtained from 1D stellar evolution calculations fairly well: a high-luminosity plateau phase and a decaying tail phase. It can be used to constrain the pre-supernova binary properties from the observed photometry of the companion star several years after the explosion in a relatively simple manner. The derived binary parameters are useful in constraining the evolutionary scenario for the progenitors and the physics of binary interactions. We apply our model to some known stripped-envelope supernova companions (SN1993J, SN2001ig, SN2006jc, SN2011dh, SN2013ge). Combined with other observational constraints such as the pre-supernova progenitor photometry, we find that SN1993J and SN2011dh likely had relatively massive companions on wide orbits, while SN2006jc may have had a relatively low-mass companion on a tight orbit. This trend suggests that type IIb supernova progenitors evolved from stable mass transfer channels and type Ibc progenitors may have formed from common-envelope channels. The constraints on orbital separation helps us probe the highly uncertain common-envelope physics for massive stars, especially with multiple epochs of companion observations. We also highlight possible limitations of our model due to the assumptions made in the underlying 1D models.

Key words: supernovae: general – binaries: general – supernovae: individual: SN1993J, SN2001ig, SN2006jc, SN2011dh, SN2013ge

1 INTRODUCTION

The vast majority of massive stars are born as members of binary or higher order multiple systems (Sana et al. 2012; Moe & Di Stefano 2017; Offner et al. 2022). Among them, the systems with relatively tight orbits are particularly interesting, as they can experience various forms of binary interactions, exchanging and/or ejecting matter from the system. This is considered to be one of the main reasons why there is a wide diversity of observational properties for core-collapse supernovae (CCSNe) (e.g. Podsiadlowski et al. 1992).

It is expected that many CCSNe are occurring with the presence of a closeby companion star, especially for stripped-envelope supernovae (SESNe), where their progenitors have lost most or all of their hydrogen-rich envelopes prior to explosion (e.g. Zapartas et al. 2017, 2019). Indeed, some companion stars have been discovered in the location of SESNe, several years after their explosions. There are five candidates detected so far: SN1993J (Maund et al. 2004; Fox et al. 2014), SN2001ig (Ryder et al. 2018), SN2006jc (Maund et al. 2016; Sun et al. 2020), SN2011dh (Maund 2019) and SN2013ge (Fox et al. 2022). We summarize the properties of the explosion and surviving companion in Table 1 and plot them on the Hertzsprung–Russell diagram (HRD) in Figure 1. While two of the companions (SN2001ig, SN2011dh) are consistent with being a main-sequence star (pink

shaded region), the other three are located within the Hertzsprung gap. This is in tension with what is typically expected, as stars only spend a very short fraction of their lives in that phase (e.g. Zapartas et al. 2017). For some of these supernovae (SNe) (SN1993J, SN2011dh) the pre-SN progenitor was also detected (Aldering et al. 1994; Maund et al. 2011; Van Dyk et al. 2011), providing critical information for understanding the evolution of the binary up to the explosion (e.g. Podsiadlowski et al. 1993; Maund et al. 2004; Benvenuto et al. 2013). However, these models are typically constructed under an implicit assumption that the companion is unaffected by the SN.

In tight binaries, the SN ejecta can collide with the companion and alter its properties. Hydrodynamical simulations show that direct mass-stripping is typically negligible when the companion is a main-sequence star ($\lesssim 1\%$; Hirai & Yamada 2015; Liu et al. 2015; Rimoldi et al. 2016; Hirai et al. 2018; Chen et al. 2023). Instead, the main effect of the SN is to heat the star through shocks, temporarily driving it out of thermal equilibrium. In response, the star can inflate and appear much cooler and more luminous than its original state (Hirai & Yamada 2015; Rimoldi et al. 2016; Hirai et al. 2018; Ogata et al. 2021b; Chen et al. 2023). This inflated state can only be maintained for a short while, and will quickly shrink back after a couple of years to decades. In Ogata et al. (2021b) we characterized this response with two parameters (the maximum luminosity and inflated duration), and found that they are strongly correlated with

★ E-mail: ryosuke.hirai@monash.edu

the mass of the companion and pre-SN orbital separation. Therefore, by observing the response of companion stars after SNe, we may be able to constrain the pre-SN orbital properties that are otherwise inaccessible.

Any empirical constraints on the pre-SN orbital separation is extremely valuable for understanding binary evolution. For example, one of the most important yet poorly understood processes in binary evolution is common-envelope evolution (Ivanova et al. 2013, 2020). In this phase, the primary star evolves and expands to engulf the companion star, leading to a rapid inspiral of the orbit and efficient mass ejection. It is recently being heavily studied in the massive star regime (e.g. Fragos et al. 2019; Law-Smith et al. 2020; Lau et al. 2022a,b; Moreno et al. 2022; Hirai & Mandel 2022), as it is considered to be responsible for explaining the origin of tight binaries involving compact objects such as X-ray binaries, SESN progenitors, gravitational wave sources, etc. Predicting the post-common-envelope orbital separation is an area of active research (Hirai & Mandel 2022; Di Stefano et al. 2023), and thus any observational constraint will be useful for distinguishing among these models.

The more stable form of mass transfer such as Roche lobe overflow is also a relatively uncertain process. Even in a steady mass transfer situation, not all the mass is retained by the accretor and part of the mass can leave the system, carrying away angular momentum. Depending on the mass retention rate and the angular momentum loss, the post-mass-transfer orbit and companion mass can vary significantly. If SESN progenitors were formed through stable mass transfer, observational constraints on pre-SN separations and the companion mass will help us understand these processes better.

In this paper, we build upon our previous work (Hirai et al. 2018; Ogata et al. 2021b) to construct a more complete model for the post-SN companion response. The key input parameters for the model are: the companion mass, companion radius, explosion energy and orbital separation. Using the properties of the observed companions to SESN progenitors, we place constraints on these input parameters. By combining this information with other observational clues, we are able to infer the history of the binary leading up to the SN.

This paper is structured as follows. We first briefly review our previous work and explain our new extended analytical model in Section 2. Results are presented in Section 3 and we discuss the implications in Section 4. We provide a summary and conclude our work in Section 5.

2 METHOD

2.1 Review of ejecta-companion interaction models

In Hirai et al. (2018) and Ogata et al. (2021b), we discovered that when the companion is a main-sequence star, it can become temporarily inflated and overluminous after being impacted by the SN ejecta of the primary star. According to our 2D hydrodynamical simulations (Hirai et al. 2018), the ejecta deposits energy into the companion through shocks, inversely proportional to the mass from the surface¹. There is a tiny amount of mass that is stripped off or ablated away, but that is usually negligible ($\lesssim 1\%$). The excess specific energy distribution in the remaining star takes the form

$$\Delta\epsilon(m) = \frac{E_{\text{heat}}}{m_{\text{h}}[1 + \ln(M_2/m_{\text{h}})]} \times \begin{cases} 1, & \text{if } m \leq m_{\text{h}}. \\ m_{\text{h}}/m, & \text{if } m > m_{\text{h}}. \end{cases} \quad (1)$$

¹ Chen et al. (2023) notes that this distribution may change for the most strongly impacted cases.

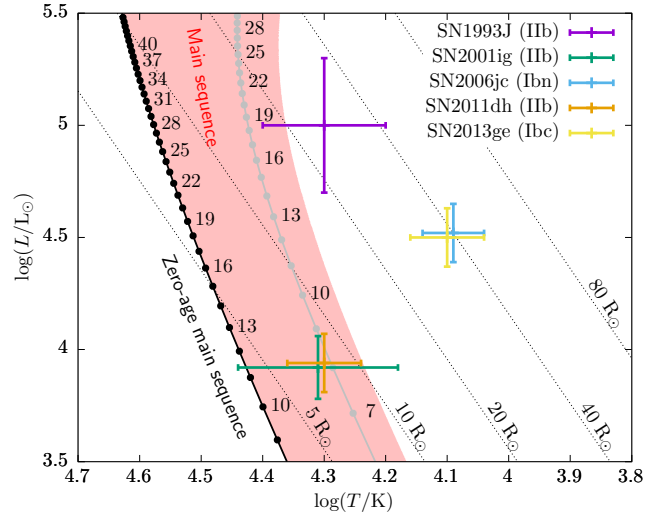


Figure 1. Location of detected SESN companions on the HRD, based on Table 1. The black curve indicates the zero-age main sequence whereas the grey curve indicates the terminal-age main sequence, and the numbers are masses in solar units. The pink shaded region shows the area that can be covered by main-sequence stars. For SN2013ge, we added error bars similar to SN2006jc for visibility.

where m is the mass from the surface, M_2 is the total companion mass, E_{heat} is the energy injected into the star, and m_{h} is a parameter that describes the efficiently heated mass. Due to the virial theorem, half of the injected energy is used for expansion and therefore only half of E_{heat} is dissipated as heat. The injected energy can be computed as $E_{\text{heat}} = p E_{\text{exp}} \tilde{\Omega}$, where p is the energy deposition efficiency, E_{exp} is the explosion energy and $\tilde{\Omega}$ is the fractional solid angle subtended by the companion described as

$$\tilde{\Omega} = \frac{1 - \sqrt{1 - (R_2/a)^2}}{2} \sim \frac{R_2^2}{4a^2}. \quad (2)$$

Here R_2 is the companion radius and a is the orbital separation. The value of the energy deposition efficiency ranges around $p \sim 0.08\text{--}0.12$, depending on how much the star gets compressed by the SN ejecta (see discussion in Section 4.3 of Hirai et al. 2018). Similarly, we found that m_{h} was related to the ejecta mass M_{ej} through $m_{\text{h}} = M_{\text{ej}} \tilde{\Omega}/2$.

Most of the excess energy is located around the surface, expanding a small amount of the surface layers to extremely large radii. Typically in our numerical experiments using the 1D stellar evolution code MESA (Paxton et al. 2011, 2013, 2015, 2018), the star stays at a fixed luminosity and radius for a few years to decades, before abruptly contracting back to close to its original size. We therefore characterized the response with two parameters: the maximum luminosity L_{max} and inflated duration τ_{inf} . We found that the maximum luminosity is almost only dependent on the companion mass M_2 through a relation

$$L_{\text{max}} = \frac{4\pi G M_2 c}{\kappa_{\text{fit}}}, \quad (3)$$

where G is the gravitational constant, and c the speed of light. This functional form is motivated by the fact that the stellar luminosity is restricted by the Eddington luminosity, except the relevant opacity is not trivial. In our 1D stellar models, the luminosity was limited by the local Eddington luminosity at the base of the near-surface convective layer, where the relevant opacity was somewhere at the edge of the

Table 1. Summary of the supernova properties and companion photometry.

Name	SN type	E_{exp} (B)	$\log(L/L_{\odot})$	$\log(T_{\text{eff}}/K)$	Epoch (yr)	Reference
SN1993J	I Ib	1–1.3	5 ± 0.3	4.3 ± 0.1	18.9	Young et al. (1995); Fox et al. (2014)
SN2001ig	I Ib	–	3.92 ± 0.14	4.31 ± 0.13	14.4	Ryder et al. (2018)
SN2006jc	I bn	~ 10	4.52 ± 0.13	4.09 ± 0.05	10.4	Tominaga et al. (2008); Sun et al. (2020)
SN2011dh	I Ib	0.6–1	3.94 ± 0.13	4.30 ± 0.06	6.3	Bersten et al. (2012); Maund (2019)
SN2013ge	I bc	1–2	~ 4.5	~ 4.1	7.0	Drout et al. (2016); Fox et al. (2022)

so-called iron bump (see discussion in Section 4.1 of Ogata et al. 2021b). We empirically set this opacity parameter κ_{fit} as

$$\kappa_{\text{fit}} = \kappa_0 \left(1 - b \frac{M_2}{M_{\odot}}\right), \quad (4)$$

where the coefficients were $\kappa_0 = 1.24 \text{ cm}^2 \text{ g}^{-1}$ and $b = 0.02$ based on fits to the maximum luminosities obtained from a large set of MESA models (Ogata et al. 2021b). The inflated state ceases once the star radiates away a fraction α of the injected energy E_{heat} . Thus the inflated duration can be approximated as

$$\tau_{\text{inf}} = \alpha \frac{E_{\text{heat}}}{L_{\text{max}}}. \quad (5)$$

We found that most of our models can be well approximated with $\alpha \sim 0.18$.

We show some examples of the luminosity evolution of the companion in Figure 2 (solid red curves). The numerical models were computed in the same way as in our previous work (Hirai et al. 2018; Ogata et al. 2021b; Ogata et al. 2021a). We choose an injection efficiency of $p = 0.08$ and all other parameters are described in each panel. The star is initially driven out of thermal equilibrium, reaching a luminosity close to the limit allowed by a star of that mass (Eq. (3)). As the star abruptly shrinks in size after τ_{inf} , the luminosity also drops abruptly by a factor of 2–3 (0.4–0.5 dex). However, it is still quite overluminous compared to its pre-heated state, as some of the energy deposited in the deeper layers diffuse out later on. The luminosity declines over a few hundred years until it regains thermal equilibrium.

2.2 Analytical model

Here we construct an analytical model to describe the full light curve of the companion including this tail part that we previously did not model. Following our previous work, we assume that no mass was stripped off and the heating of the companion by the SN is instantaneous. A fraction of the SN energy is deposited into the star with a distribution following Eq. (1). The star then tries to get rid of this excess heat by transporting it outwards. We assume a very simple picture where the excess energy is transported outwards in mass coordinate with some timescale τ_{tr} that is universal over the entire star. It can be considered as carrying the excess energy on a conveyor belt, where the energy that reaches the end of the conveyor belt (= stellar surface) is emitted as radiation. The conveyor belt completes one cycle over the time τ_{tr} . Under this assumption, the surface excess luminosity at a given time can be described as

$$L_{\text{ex}}(t) = \frac{\Delta\epsilon(M_2 t / \tau_{\text{tr}}) M_2}{2\tau_{\text{tr}}}. \quad (6)$$

The term $\Delta\epsilon(M_2 t / \tau_{\text{tr}})$ indicates which part of the initial excess energy distribution has reached the surface. This specific energy is multiplied by M_2 and divided by the transport timescale τ_{tr} to obtain

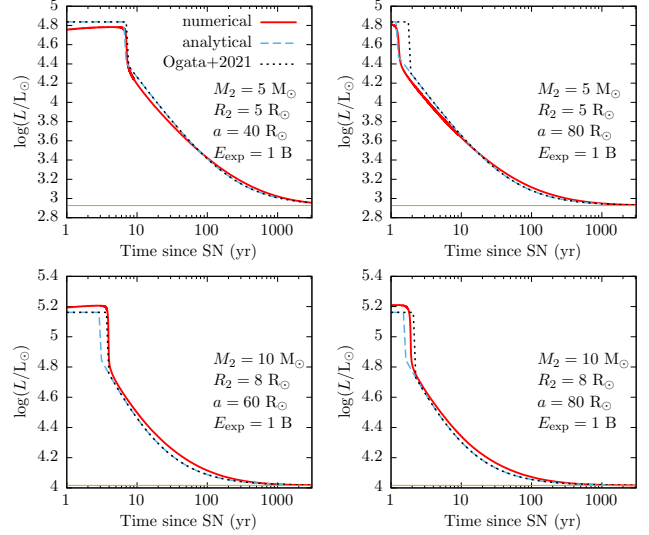


Figure 2. Light curves of the companion response to SN heating. Each panel shows results for different binary and explosion parameters. Red solid curves are from simulations with MESA and the black dashed curves are from our analytical model. The orange lines mark the luminosity of the companion before the SN impact.

the rate at which the excess energy escapes the star. Note that the factor two in the denominator comes from an assumption that half of the luminosity is used as thermodynamic work to maintain the inflated stellar structure. However, the star does not radiate at luminosities higher than the maximum allowed value given in Eq. (3) in our MESA models. Hence the luminosity is initially capped by L_{max} until the total radiated energy exceeds the integrated energy excess from the surface down to $m = M_2 t / \tau_{\text{tr}}$. It is analogous to having a “waiting list” for the excess heat to escape out, and the flux remains constant until the waiting list is exhausted. Once the waiting list is exhausted, the luminosity is determined by the amount of excess heat at the surface, as expressed in Eq. (6). The full light curve can thus be expressed as

$$L_2(t, M_2, E_{\text{heat}}) = \begin{cases} L_{\text{max}}(M_2), & \text{if } t \leq \tau_{\text{inf}}. \\ \frac{E_{\text{heat}}}{2[1 + \ln(M_2/m_h)]} \cdot \frac{1}{t} + L_{\text{org}}, & \text{if } t > \tau_{\text{inf}}. \end{cases} \quad (7)$$

where $L_{\text{org}} = L_{\text{org}}(M_2)$ is the luminosity of the companion prior to being heated.

The only model parameter that needs to be determined is the transport timescale τ_{tr} . Interestingly, it does not appear in Eq. (7) except implicitly in the definition of τ_{inf} . The τ_{tr} -dependence cancels out due to the heat excess distribution being proportional to $\Delta\epsilon \propto 1/m$

in Eq. (1). This makes our light curve model rather robust to model assumptions at least for the tail part. We roughly estimate τ_{tr} as

$$\tau_{\text{tr}} \sim \frac{GM_2^2}{2R_2L_{\text{max}}(M_2)}, \quad (8)$$

which is similar to the thermal timescale of the star, except evaluated with the maximum luminosity. The inflated timescale can then be obtained by finding the larger root of the following equation for τ_{inf}

$$(L_{\text{max}} - L_{\text{org}})\tau_{\text{inf}} = \frac{E_{\text{heat}}}{2[1 + \ln(M_2/m_h)]} \left(1 + \ln \frac{M_2\tau_{\text{inf}}}{m_h\tau_{\text{tr}}} \right), \quad (9)$$

when

$$L_{\text{max}} > \frac{E_{\text{heat}}M_2}{2[1 + \ln(M_2/m_h)]\tau_{\text{tr}}m_h} + L_{\text{org}}. \quad (10)$$

If Eq. (10) is not satisfied, the star never approaches $L_2 = L_{\text{max}}$ so $\tau_{\text{inf}} = 0$. Note that this analytical framework is designed to mimic the results of our MESA models, so it is bound by the same uncertainties that the underlying 1D models have. The degree of inflation and τ_{inf} can contain large uncertainties as explained in Section 4.2.

For the companion radius R_2 and luminosity L_{org} , we use the analytical fits by [Hurley et al. \(2000\)](#) for main-sequence stars, assuming an age $t_{\text{age}} \sim 10$ Myr, which roughly corresponds to the lifetime of a $20 M_{\odot}$ star. This assumes that the companion is coeval with the SN progenitor and has not been rejuvenated by mass accretion. In reality, the companion may have accreted a substantial amount of mass depending on the preceding evolution, and our stellar radii and luminosity estimates may be incorrect. However, given the uncertainty in the progenitor mass (and thus companion age) and explosion energy, we ignore the errors on our companion property estimates.

3 RESULTS

We compare this analytic light curve model (dashed curves) against the numerical models (solid curves) in Figure 2. Most remarkably, the tail part of the light curves display an almost perfect match for all the models shown. This demonstrates the validity of our model despite having many simplifying assumptions. For the plateau phase, we have recalibrated our fitting coefficients for L_{max} to $\kappa_0 = 1 \text{ cm}^2 \text{ g}^{-1}$ and $b = 0.01$ (it was $\kappa_0 = 1.24 \text{ cm}^2 \text{ g}^{-1}$ and $b = 0.02$ in [Ogata et al. 2021b](#)). With this recalibration, the analytical models show good agreement with the numerical models for L_{max} within the parameter space we explored. As for the duration of the plateau phase, our estimates based on Eqs. (8)–(9) seem to explain the numerical models relatively well although in many cases it slightly underestimates. As reference, we overplot some models estimating the inflated timescale with the empirical fit as in Eq. (5) (dotted curves). In both cases, the light curve in the tail phase are treated identically.

In Figure 3, we plot a set of analytical light curves that satisfy the observational constraint for the companion of SN2013ge ([Fox et al. 2022](#)). We assumed $E_{\text{exp}} = 1.5 \text{ B}$, based on the observationally inferred explosion energy (see Table 1). There are two different ways to fit the single observed point, depending on which part of the light curve it is fitted in: the plateau phase or the tail phase.

The green curves were computed assuming the observed companion is in the plateau phase. Since the luminosity of the plateau phase only depends on the companion mass, the luminosity provides a unique constraint on the companion mass as $M_2 = 2.36 M_{\odot}$. The pre-SN orbital separation and explosion energy determines the duration of the plateau phase. Two light curves computed with the minimum and maximum possible orbital separations are shown, but

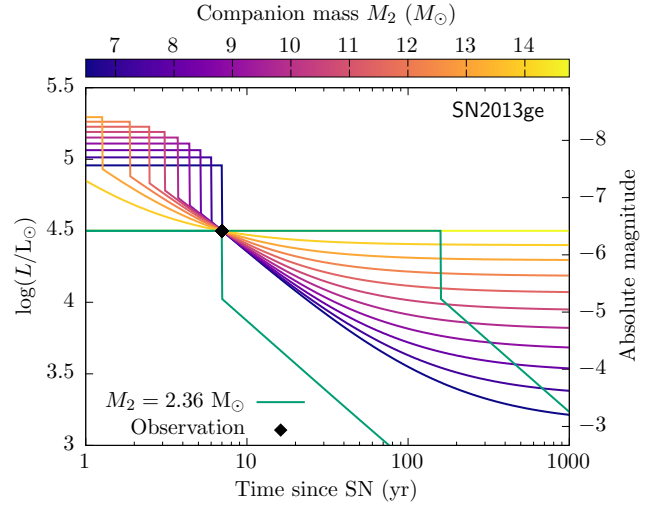


Figure 3. Companion response light curves that satisfy the current observed companion photometric constraints of SN2013ge (Black diamond). We assumed $E_{\text{exp}} = 1.5 \text{ B}$ and $M_2 = 4.5 M_{\odot}$. The green curves are example light curves fitted to the observation in the plateau phase with a companion mass of $M_2 = 2.36 M_{\odot}$ and two different orbital separations. The right (left) curve is computed with the minimum (maximum) orbital separation (see text for details). All other curves are computed by fitting the observation in the tail phase.

any curve in between are also possible. The physically possible minimum separation is where the companion radius equals its Roche lobe radius, whereas the maximum separation is when the plateau phase duration is equal to the observed epoch for the companion star. To compute the Roche lobe radius, we assumed a progenitor mass of $M_1 = 4.5 M_{\odot}$, which produces an ejecta mass consistent with the typical observed value for SESNe ($M_{\text{ej}} \sim 3 M_{\odot}$; [Lyman et al. 2016](#); [Taddia et al. 2018](#); [Prentice et al. 2019](#)). At the minimum separation, the inflated duration can be as long as ~ 150 yr.

All other curves were fitted in the tail phase. A different combination of a and M_2 is required for each curve to fit the observed point. The minimum possible mass in this regime is $M_2 \sim 6.5 M_{\odot}$, and can reach as high as $M_2 \sim 14.8 M_{\odot}$. Depending on the mass, the light curve will have a different decline rate and thus predict different luminosities 10 yr from now. With another epoch of observations, we will be able to constrain the true companion mass and pre-SN orbital separation at the same time. In Appendix A, we show similar plots fitted to the observed companions for the other SNe listed in Table 1.

Figure 4 shows the constraints on the allowed combinations of a and M_2 based on our light curve fits to observed companions. The vertical bars with triangles denote the allowed range for pre-SN separations when fitted to the plateau phase. Solid parts of the curves indicate the constraints when fitted to the tail phase, whereas the dashed parts are fitted exactly at the location of the jump. All curves have similar shapes extending from the bottom left to top right. Basically, the current photometry can be explained by either a low-mass companion in a tight pre-SN orbit or a high-mass companion in a wide orbit. At the highest masses, the equilibrium luminosity L_{org} approaches the observed luminosity. At this limit, we can only place lower limits on the pre-SN separation based on the fact that the companion is essentially unheated ([Rizzo Smith et al. 2023](#)).

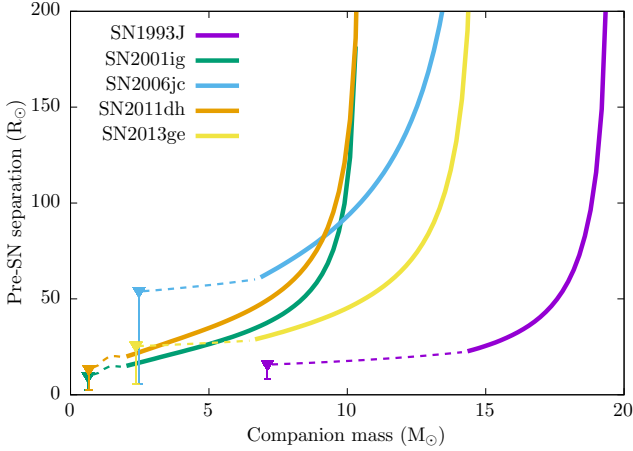


Figure 4. Constraints on the pre-SN orbital separations. Here we assumed the progenitor had a lifetime of 8.7 Myr. Solid parts of the curves are based on fits to the tail phase. The vertical bars are based on fits to the plateau phase. The dashed parts of the curves are based on fits to the jump between the plateau and tail phases.

4 DISCUSSION

4.1 Additional constraints

In the previous section, we have only used a single post-SN companion photometric constraint to infer the pre-SN binary properties. For some of the SNe we have additional observational constraints that help us partially break the degeneracy.

4.1.1 Pre-SN photometry

SN1993J and SN2011dh have pre-SN progenitor detections in addition to the companion. The size of stars inferred from the photometry can be used to rule out part of the parameter space, as the progenitor should have been contained within its Roche lobe prior to explosion. Roughly speaking, the separation should be ≥ 3 times larger than the stellar radius in order to fit in a star within its Roche lobe, although the exact value depends on the mass ratio (Eggleton 1983). Here we show that even the loosest constraint of $a > R_2$ is sufficient to rule out significant amounts of parameter space.

The pre-explosion photometry of SN1993J is consistent with a K-supergiant with $\log(L/L_\odot) = 5.1 \pm 0.3$ and $\log(T/K) = 3.63 \pm 0.05$ (Maund et al. 2004). This corresponds to a radius of $\sim 650 R_\odot$, meaning the pre-SN separation had to be at least $a > 650 R_\odot$. At such wide separations, the SN ejecta has little impact on the companion, and should look like a regular star. According to Figure 4, the companion mass should be $M_2 \sim 19\text{--}20 M_\odot$ if the pre-SN separation was $> 650 R_\odot$.

Similarly, the progenitor of SN2011dh is consistent with being an F-supergiant with $\log(L/L_\odot) = 4.92 \pm 0.20$ and $T = 6000 \pm 260$ K (Maund et al. 2011; Van Dyk et al. 2011), with a corresponding radius of $R_2 \sim 270 R_\odot$. This again is a sufficiently large value that the SN ejecta would have little impact on the companion radius. The inferred companion mass would then be $\sim 10 M_\odot$, based on Figure 4.

4.1.2 Multiple epochs of companion detections

Our analytical constraints on the pre-SN binary properties were placed based on one epoch of post-SN observations (Table 1). Some

of the SNe already have a second epoch of observations, which can be used to pin down the pre-SN binary parameters to a single combination.

SN1993J is one of the best observed SNe aside from SN1987A, and has multiple late-time observations. The putative hot companion was first detected in 2003, with near-UV spectra suggesting the existence of a B-supergiant (Maund et al. 2004). It was later followed up in 2004–2006 (Maund & Smartt 2009) and 2012 (Fox et al. 2014), confirming the hot B star contribution. Although the SN and companion have not been fully disentangled, the B star contribution seems to be constant over the multiple epochs. This supports the scenario above that the companion is a relatively massive star ($M_2 \sim 19 M_\odot$) on a wide orbit such that it does not get strongly impacted by the SN.

SN2006jc is another object with multiple late-time observations. The first observation of the companion was made ~ 3.6 yr after the explosion (Maund et al. 2016), whereas the second observation was ~ 10.4 yr after the explosion (Sun et al. 2020). Different filter combinations were used in each epoch making it difficult to provide a direct comparison, but generally the fluxes were consistent with being the same object. If this is true, only the two ends of the solution space remain: a low-mass companion ($M_2 = 2.47 M_\odot$) on a tight orbit ($a \lesssim 50 R_\odot$) or a high-mass companion ($M_2 \sim 15 M_\odot$) on a wide orbit ($a \gtrsim 200 R_\odot$). Both solutions are viable, but the fact that the companion has a temperature off the main sequence (Fig 1) supports the case that the star was somehow affected by the SN. While it is not impossible to have a companion star that happens to be in the Hertzsprung gap, it is quite rare and requires a rather fine-tuned initial mass ratio. Therefore, we argue that the companion is more likely to have been a heated low-mass star rather than an unscathed high-mass star. Having an evolved companion also makes it prone to mass stripping by the SN (Hirai et al. 2014, 2020), and thus using our current analytical model is misleading.

4.2 Caveats

In our analytical model, we only modelled the luminosity evolution and ignored the radius/temperature response. Our previous 1D simulations show that the radius can be greatly inflated during the plateau phase and quickly contracts after the luminosity drop. Therefore, the star only stays in the Hertzsprung gap region for a relatively short time. It may thus be difficult to explain the exact photometry of observed companions as displayed in Figure 1. In Ogata et al. (2021b), we proposed that interactions with the new-born neutron star may be able to keep a star in the Hertzsprung gap region if the binary can survive. The current radius may then be a measure of the current orbit periapsis or the Roche lobe radius.

The stellar radii of these temporarily out-of-equilibrium stars are also very sensitive to the outer boundary conditions. Since the luminosity of the surface layers of the heated star is close to the Eddington limit, the 1D models computed based on hydrostatic equilibrium are not completely reliable. The high luminosity may drive non-spherical effects, altering the effective opacity distribution as we discuss later. Alternatively, the high luminosity may drive a “superwind”, getting rid of the excess energy in the form of mass loss and not radiation (Vassiliadis & Wood 1993). In strongly mass-losing situations, the outer boundary becomes dynamical and the hydrostatic assumption breaks down (Poniatowski et al. 2021). Inflated envelopes may be subject to pulsational instabilities, causing strong radial pulsations (Sanyal et al. 2015). All of these effects could influence the stellar structure in the outer parts, and could alter the stellar radius significantly. In some cases the slower parts of the SN ejecta may be captured by the companion, partly obscuring the light or adding to the

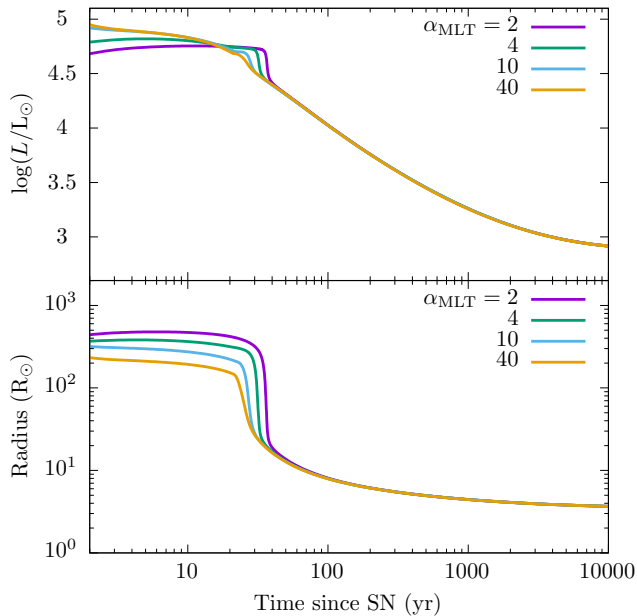


Figure 5. Comparison of the stellar response with different mixing lengths applied for convection. The adopted model parameters were $M_2 = 5M_\odot$, $R_2 = 3.5R_\odot$, $E_{\text{exp}} = 1B$, $\alpha = 13R_\odot$.

extinction. Such complications make it difficult to accurately model the radius/temperature evolution of the post-SN companions.

The existence of both the inflated state and the maximum luminosity are strongly correlated. Inflated envelopes are known to emerge as a consequence of inefficient near-surface convection (Sanyal et al. 2015). This is likely due to the way convection is treated in 1D stellar evolution codes. In reality, other potential modes of energy transport may arise such as waves excited by turbulent convection (e.g. Maeder 1987) or developing porous layers that reduce the effective opacity (e.g. Shaviv 1999; Begelman 2001; Owocki et al. 2004). To test how extra modes of energy transport may influence our models, we performed the same MESA calculation with different energy transport efficiencies by changing the mixing length parameter α_{MLT} . In Figure 5, we compare the light curve and radius evolution for various mixing lengths. As we increase the mixing length, the maximum achieved luminosity increases while the plateau phase shortens. At the same time, the radius during the inflated phase decreases with larger mixing lengths. However, both the luminosity and radius evolution are identical during the tail phases. We therefore believe that if the main effect of near-Eddington luminosities in stars is to activate more efficient energy transport mechanisms, our bolometric light curve models are still valid especially for the tail phase where the luminosity is sufficiently sub-Eddington. Within our framework, this can be regarded as an uncertainty in L_{max} and τ_{inf} . On the other hand, if the high luminosity leads to enhanced winds, dynamical pulsations or eruptions, the results may differ in less trivial ways.

The explosion energy for SN2006jc is highly uncertain. Here, we used the observationally inferred value $E_{\text{exp}} = 10B$ (Tomimaga et al. 2008), which is an order of magnitude higher than the typical energies for SNeIb. This was calculated under the assumption that the SN light curve was powered mostly by radioactive decay. However, it is known that there was some degree of interaction between the SN ejecta and dense circumstellar material (CSM) from its narrow

He I lines and X-ray emission (Brown et al. 2006; Immler et al. 2006, 2008). Depending on how much the CSM-interaction contributed to the light curve, the explosion energy estimate could be substantially overestimated. Our constraints on the pre-SN separation (Fig 4) can be much lower depending on what the true explosion energy is.

4.3 Implications for SESN progenitor formation channels

The two main channels in creating stripped-envelope stars in binaries are via stable mass transfer and common-envelope evolution. Both channels are expected to be contributing to the whole population of SESNe (Podsiadlowski et al. 1992). However, the dominant channel may differ depending on each SN subtype, which have differing degrees of remaining hydrogen. Stable mass transfer ceases when the star loses a significant fraction of its envelope and contracts to detach from its Roche lobe. There is still some hydrogen left on top of its core at this point, and the amount depends on the orbital separation and metallicity (Ouchi & Maeda 2017; Laplace et al. 2020). Depending on the subsequent wind mass loss and/or later mass transfer episodes, the star may or may not get rid of this remaining hydrogen. Therefore, stable mass transfer channels can create both SNIbc and SNIib progenitors (Yoon et al. 2017). On the other hand, common-envelope channels are expected to end up with much tighter separations, leaving little to no space for any hydrogen to remain. This implies that common-envelope channels may contribute to the SNIbc population but not much to the SNIib progenitors. However, a recent model for massive star common-envelopes suggest much wider separations depending on the companion mass, allowing for possible SNIib progenitor formation² (Hirai & Mandel 2022).

Another distinguishing feature between the two channels is the companion mass. Whether or not the binary undergoes a stable or unstable mass transfer phase depends on many factors such as the evolutionary stage of the donor, mass ratio, the companion star properties, etc (e.g. Hjellming & Webbink 1987). The exact dividing line depends on many uncertain physics such as the response of the star to mass loss (Soberman et al. 1997; Pavlovskii & Ivanova 2015; Temmink et al. 2023) and the dynamics of the mass ejected from the system (e.g. MacLeod et al. 2018). However, it is qualitatively true that lower mass companions lead to more unstable mass transfer and will experience common-envelope phases. Therefore, post-common-envelope systems will have lower mass companions compared to systems that experienced stable mass transfer. Additionally, stable mass transfer proceeds over a longer timescale, allowing the companion to accrete more material and grow in mass.

The constraints placed on the pre-SN binary parameters in the previous section are useful in figuring out which channel formed each SN progenitor. For example, the two SNeIib SN1993J and SN2011dh are constrained to have relatively massive secondaries on wide orbits (Section 4.1.1). Therefore, the progenitor system of SN1993J and SN2011dh likely evolved via stable mass transfer channels. This is in line with various binary evolution modelling attempts for these systems (e.g. Podsiadlowski et al. 1993; Maund et al. 2004; Benvenuto et al. 2013). Additionally, the SNeIib companion photometry are consistent with being on the main sequence (Fig 1), strengthening the case that these stars were not heated by the SN impact.

For SN2006jc, our model predicts that the companion mass can be as low as $M_2 \sim 2.5M_\odot$, which is too low to sustain a stable mass transfer phase so it likely experienced a common-envelope phase. If

² See also Naiman et al. (2020); Shishkin & Soker (2020) on models involving grazing envelope evolution.

the companion luminosity fades over the next few decades, it will confirm that the companion is a lower mass star, supporting the common-envelope scenario. In our analysis, the pre-SN separation, which is directly related to the post-common-envelope separation, is $\lesssim 55 R_{\odot}$ (Figure 4). The upper edge is somewhat wider than what is typically predicted from the classical energy formalism for common-envelope evolution (e.g. Webbink 1984). Therefore, if the companion turns out to be a lower mass star, it will provide strong support for the recent claims that common-envelope phases are much more efficient at ejecting their envelopes in the massive star regime (Fragos et al. 2019; Hirai & Mandel 2022).

The other two SNe on our list do not have additional constraints to help break the degeneracy. However, given that SN2001ig has a very similar companion photometry to SN2011dh, and SN2013ge is similar to SN2006jc (Fig 1), it is tempting to associate them as having similar histories. If this speculation is true, it gives rise to an interesting trend: all the SNeIb in this list experienced stable mass transfer and the SNeIbc experienced common-envelope phases. It is not appropriate to draw strong conclusions from this small sample size but this trend supports the idea that the distinction between SNIb and SNIbc progenitors is more related to the mode of binary interaction it experienced than other factors such as mass or metallicity (Fang et al. 2019; Sun et al. 2023). Another epoch of companion photometry within the next decade or so will be useful in confirming the true identities of these stars and their evolutionary histories.

5 SUMMARY AND CONCLUSION

We present a convenient analytical framework that describes the photometric response of companion stars after being impacted by SNe. The relatively simple form of the model allows us to solve the inverse problem, i.e. we can infer the pre-SN binary properties given the post-SN companion observations.

As a demonstration of how our formula can be used to constrain binary interaction physics, we applied our model to five SESNe that have post-SN companion detections (SN1993J, SN2001ig, SN2006jc, SN2011dh, SN2013ge). With one epoch of observations, we are able to place a constraint on the relation between the companion mass and pre-SN orbital separation. Combined with other constraints such as the pre-SN progenitor photometry and/or post-SN companion photometry for multiple epochs, we can determine the evolutionary history of the progenitor system. Based on our analysis, we find that two of the SNeIb (SN1993J, SN2011dh) most likely had a fairly massive companion and evolved via stable mass transfer, supporting previous modelling attempts (Podsiadlowski et al. 1993; Maund et al. 2004; Benvenuto et al. 2013). For the SNIbn 2006jc, we argue that it likely had a lower-mass companion and evolved through a common-envelope phase.

While this framework is useful for rough and quick interpretations from observations, extra work is required to fully understand the response of companion stars after SNe. Our formula hinges on several key assumptions. First, we assume the amount of stripped mass from the companion is negligible. This is generally not a bad assumption, but can sometimes be large enough to influence the long-term response (Hirai et al. 2018; Chen et al. 2023). Secondly, we rely on MESA calculations as a basis of our analytical model. Because of the extreme near-Eddington luminosities and non-equilibrium nature of SN-heated stars, the intrinsic approximations are inappropriate in some regimes (Section 4.2). Further detailed modelling of near-Eddington envelopes is required to predict the accurate response of SN-impacted companions.

Continued monitoring of the companions over the next few decades can help pin down the pre-SN orbital separations, which is a vital constraint not only to determine their formation channels, but also for understanding binary interaction physics such as the common-envelope phase mechanism and mass transfer efficiency. Such constraints can ultimately help us understand the formation of other objects including X-ray binaries and gravitational wave sources.

In addition to the five SNe we studied, SN2016gkg may be another interesting source (Kilpatrick et al. 2022) to continue monitoring. This SNIb has faded below the pre-SN source but now has excess emission that could indicate a surviving companion. Together with its rich information including the progenitor photometry (Tartaglia et al. 2017; Kilpatrick et al. 2017) and early light curve (Arcavi et al. 2017; Bersten et al. 2018), we will be able to work out its evolutionary origin.

ACKNOWLEDGEMENTS

The author thanks Alexander Heger and Team COMPAS for useful discussions. The author also thanks the anonymous referee for insightful comments that improved the manuscript. RH is supported by the Australian Research Council (ARC) Centre of Excellence for Gravitational Wave Discovery (OzGrav), through project number CE170100004.

DATA AVAILABILITY

The data underlying this article will be shared on reasonable request to the corresponding author.

REFERENCES

- Aldering G., Humphreys R. M., Richmond M., 1994, *AJ*, **107**, 662
 Arcavi I., et al., 2017, *ApJ*, **837**, L2
 Begelman M. C., 2001, *ApJ*, **551**, 897
 Benvenuto O. G., Bersten M. C., Nomoto K., 2013, *ApJ*, **762**, 74
 Bersten M. C., et al., 2012, *ApJ*, **757**, 31
 Bersten M. C., et al., 2018, *Nature*, **554**, 497
 Brown P. J., Immler S., Modjaz M., 2006, *The Astronomer's Telegram*, **916**, 1
 Chen H.-P., Rau S.-J., Pan K.-C., 2023, *ApJ*, **949**, 121
 Di Stefano R., Kruckow M. U., Gao Y., Neunteufel P. G., Kobayashi C., 2023, *ApJ*, **944**, 87
 Drout M. R., et al., 2016, *ApJ*, **821**, 57
 Eggleton P. P., 1983, *ApJ*, **268**, 368
 Fang Q., Maeda K., Kuncarayakti H., Sun F., Gal-Yam A., 2019, *Nature Astronomy*, **3**, 434
 Fox O. D., et al., 2014, *ApJ*, **790**, 17
 Fox O. D., et al., 2022, *ApJ*, **929**, L15
 Fragos T., Andrews J. J., Ramirez-Ruiz E., Meynet G., Kalogera V., Taam R. E., Zezas A., 2019, *ApJ*, **883**, L45
 Hirai R., Mandel I., 2022, *ApJ*, **937**, L42
 Hirai R., Yamada S., 2015, *ApJ*, **805**, 170
 Hirai R., Sawai H., Yamada S., 2014, *ApJ*, **792**, 66
 Hirai R., Podsiadlowski Ph., Yamada S., 2018, *ApJ*, **864**, 119
 Hirai R., Sato T., Podsiadlowski Ph., Vigna-Gómez A., Mandel I., 2020, *MNRAS*, **499**, 1154
 Hjellming M. S., Webbink R. F., 1987, *ApJ*, **318**, 794
 Hurley J. R., Pols O. R., Tout C. A., 2000, *MNRAS*, **315**, 543
 Immler S., Modjaz M., Brown P. J., 2006, *The Astronomer's Telegram*, **934**, 1
 Immler S., et al., 2008, *ApJ*, **674**, L85

Ivanova N., et al., 2013, *A&ARv*, 21, 59
Ivanova N., Justham S., Ricker P., 2020, Common Envelope Evolution, doi:10.1088/2514-3433/abb6f0.
Kilpatrick C. D., et al., 2017, *MNRAS*, 465, 4650
Kilpatrick C. D., Coulter D. A., Foley R. J., Piro A. L., Rest A., Rojas-Bravo C., Siebert M. R., 2022, *ApJ*, 936, 111
Laplace E., Göteborg Y., de Mink S. E., Justham S., Farmer R., 2020, *A&A*, 637, A6
Lau M. Y. M., Hirai R., González-Bolívar M., Price D. J., De Marco O., Mandel I., 2022a, *MNRAS*, 512, 5462
Lau M. Y. M., Hirai R., Price D. J., Mandel I., 2022b, *MNRAS*, 516, 4669
Law-Smith J. A. P., et al., 2020, *arXiv e-prints*, p. arXiv:2011.06630
Liu Z.-W., Tauris T. M., Röpké F. K., Moriya T. J., Kruckow M., Stancliffe R. J., Izzard R. G., 2015, *A&A*, 584, A11
Lyman J. D., Bersier D., James P. A., Mazzali P. A., Eldridge J. J., Fraser M., Pian E., 2016, *MNRAS*, 457, 328
MacLeod M., Ostriker E. C., Stone J. M., 2018, *ApJ*, 868, 136
Maeder A., 1987, *A&A*, 173, 247
Maund J. R., 2019, *ApJ*, 883, 86
Maund J. R., Smartt S. J., 2009, *Science*, 324, 486
Maund J. R., Smartt S. J., Kudritzki R. P., Podsiadlowski Ph., Gilmore G. F., 2004, *Nature*, 427, 129
Maund J. R., et al., 2011, *ApJ*, 739, L37
Maund J. R., Pastorello A., Mattila S., Itagaki K., Boles T., 2016, *ApJ*, 833, 128
Moe M., Di Stefano R., 2017, *ApJS*, 230, 15
Moreno M. M., Schneider F. R. N., Röpké F. K., Ohlmann S. T., Pakmor R., Podsiadlowski Ph., Sand C., 2022, *A&A*, 667, A72
Naiman B. V., Sabach E., Gilkis A., Soker N., 2020, *MNRAS*, 491, 2736
Offner S. S. R., Moe M., Kratter K. M., Sadavoy S. I., Jensen E. L. N., Tobin J. J., 2022, *arXiv e-prints*, p. arXiv:2203.10066
Ogata M., Hirai R., Hijikawa K., 2021a, The observability of inflated companion stars after supernovae in massive binaries, doi:10.5281/zenodo.4624586, https://doi.org/10.5281/zenodo.4624586
Ogata M., Hirai R., Hijikawa K., 2021b, *MNRAS*, 505, 2485
Ouchi R., Maeda K., 2017, *ApJ*, 840, 90
Owocik S. P., Gayley K. G., Shaviv N. J., 2004, *ApJ*, 616, 525
Pavlovskii K., Ivanova N., 2015, *MNRAS*, 449, 4415
Paxton B., Bildsten L., Dotter A., Herwig F., Lesaffre P., Timmes F., 2011, *ApJS*, 192, 3
Paxton B., et al., 2013, *ApJS*, 208, 4
Paxton B., et al., 2015, *ApJS*, 220, 15
Paxton B., et al., 2018, *ApJS*, 234, 34
Podsiadlowski Ph., Joss P. C., Hsu J. J. L., 1992, *ApJ*, 391, 246
Podsiadlowski Ph., Hsu J. J. L., Joss P. C., Ross R. R., 1993, *Nature*, 364, 509
Poniatowski L. G., et al., 2021, *A&A*, 647, A151
Prentice S. J., et al., 2019, *MNRAS*, 485, 1559
Rimoldi A., Portegies Zwart S., Rossi E. M., 2016, *Computational Astrophysics and Cosmology*, 3, 2
Rizzo Smith M., Kochanek C. S., Neustadt J. M. M., 2023, *MNRAS*, 523, 1474
Ryder S. D., et al., 2018, *ApJ*, 856, 83
Sana H., et al., 2012, *Science*, 337, 444
Sanyal D., Grassitelli L., Langer N., Bestenlehner J. M., 2015, *A&A*, 580, A20
Shaviv N. J., 1999, *Phys. Rep.*, 311, 177
Shishkin D., Soker N., 2020, *MNRAS*, 497, 855
Soberman G. E., Phinney E. S., van den Heuvel E. P. J., 1997, *A&A*, 327, 620
Sun N.-C., Maund J. R., Hirai R., Crowther P. A., Podsiadlowski Ph., 2020, *MNRAS*, 491, 6000
Sun N.-C., Maund J. R., Crowther P. A., 2023, *MNRAS*, 521, 2860
Taddia F., et al., 2018, *A&A*, 609, A136
Tartaglia L., et al., 2017, *ApJ*, 836, L12
Temmink K. D., Pols O. R., Justham S., Istrate A. G., Toonen S., 2023, *A&A*, 669, A45
Tominaga N., et al., 2008, *ApJ*, 687, 1208

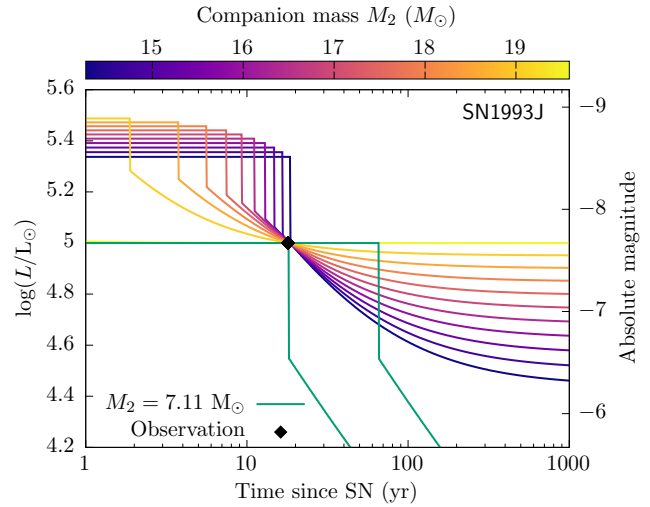


Figure A1. Same as Fig. 3 but for SN1993J.

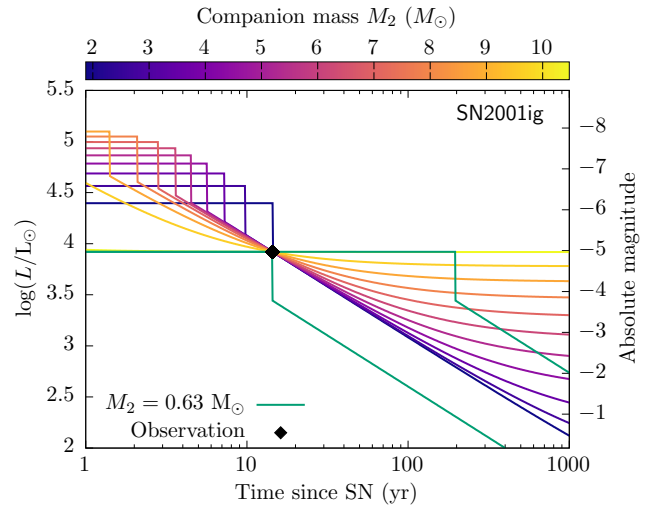


Figure A2. Same as Fig. 3 but for SN2001ig.

Van Dyk S. D., et al., 2011, *ApJ*, 741, L28
Vassiliadis E., Wood P. R., 1993, *ApJ*, 413, 641
Webbink R. F., 1984, *ApJ*, 277, 355
Yoon S.-C., Dessart L., Clocchiatti A., 2017, *ApJ*, 840, 10
Young T. R., Baron E., Branch D., 1995, *ApJ*, 449, L51
Zapartas E., et al., 2017, *ApJ*, 842, 125
Zapartas E., et al., 2019, *A&A*, 631, A5

APPENDIX A: OTHER LIGHT CURVES

Figures A1–A4 show the same plots as Figure 3 but for the companion photometry of SN1993J, SN2001ig, SN2006jc and SN2011dh as listed in Table 1. For the explosion energy, we used the median value within the observationally inferred range (Table 1). For SN2001ig, the peak of the light curve was not observed so there are no good constraints on the explosion energy. We simply use the canonical value $E_{\text{exp}} = 1 \text{ B}$ for SN2001ig.

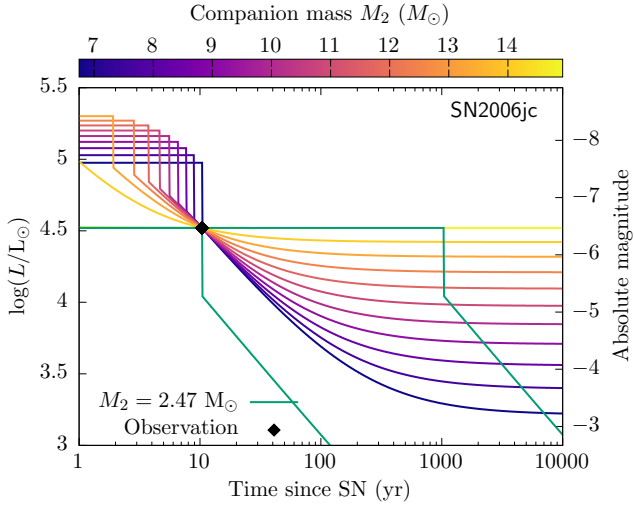


Figure A3. Same as Fig. 3 but for SN2006jc.

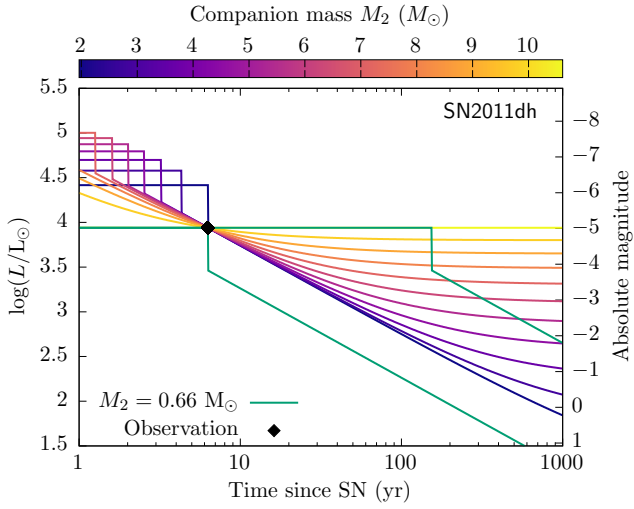


Figure A4. Same as Fig. 3 but for SN2011dh.

This paper has been typeset from a \LaTeX file prepared by the author.